

Simulation of Three-Sided Lid-Driven Cavity

Abanoub G. Kamel, Eman H. Haraz, and Sarwat N. Hanna

Abstract—In this paper, an incompressible, two-dimensional (2D), time-dependent, and laminar Newtonian fluid flow in a square cavity is simulated in order to investigate vortex dynamics in cavities. Navier-Stokes equations in vorticity-stream function formulation are solved numerically using the finite difference method (FDM) and alternating direction implicit (ADI) technique as they are computationally effective. Two original, distinguished, and unexplored cases of the three-sided lid-driven cavity have been investigated. In case (1) the upper and lower walls are translated to the right whereas the left wall is translated upward and the right wall remains stationary. Furthermore, in case (2) the upper wall is translated to the right but the lower wall is translated to the left whereas the left wall is translated downward and the right wall remains stationary. Moreover, the speed magnitude is unity for all moving walls. However, a MATLAB[®] code is developed, used, and validated by studying the one-sided lid-driven cavity. The results were in a very good agreement. Besides, stream function and vorticity values in addition to the location of primary and secondary vortices' centers inside the square cavity have been revealed at low and intermediate Reynolds numbers, typically ($Re=100$ to 2000). Moreover, as Reynolds number increases, more secondary vortices are generated near the cavity corners and the main primary vortex approaches the cavity center.

Index Terms—Finite difference method, lid-driven cavity, navier-stokes equations, vorticity-stream function formulation.

I. INTRODUCTION

Since the mid of the past century, the flow inside a 2D lid-driven square cavity was an interesting research field for several fluid dynamics investigators as it serves as a benchmark problem. Also, it is popular due to its simple geometry and the importance of studying vortices formation and location as well as the flow inside containers especially at the corners where cavitation occurs. The objective of solving this problem relies on its importance in several industrial applications such as short-dwell coaters utilized for the manufacturing of high-quality photographic films and papers, roll coating, several color printings, polymer processing apparatus design, Bingham plastics flows, dryers, and solar collectors [1]-[6].

Ghadimi et al. [7] simulated the flow in a square as well as the L-shaped cavity using fourth-order FDM. There are two review articles on the lid-driven cavity flows stated in [8] and [9] for all curious readers. The accuracy can be achieved by choosing an appropriate mathematical technique for solving the Navier-Stokes equations. However, they will be solved

numerically in vorticity-stream function formulation ($\psi-\omega$) for incompressible, 2D fluid flow using Finite Difference Method (FDM) and an implicit technique known as Alternating Direction Implicit (ADI) scheme as stated by Peaceman and Rachford, Jr [10]. One-sided, two-side and four-sided lid-driven cavity flows have been studied in these articles [11] and [12] because of the rapid evolution of cavity flows. However, a MATLAB[®] code is developed, used, and validated by studying the one-sided lid-driven cavity at ($Re = 2000$) and the results were compared with Gupta and Kalita [13] and they were in a very good agreement. Unlike two-sided and four-sided lid driven cavities, the three-sided lid driven cavity has no symmetry about any of its axes. The aim of the present study is to investigate the three-sided lid-driven cavity since it was not studied previously besides its academic value for vortices dynamics at corners.

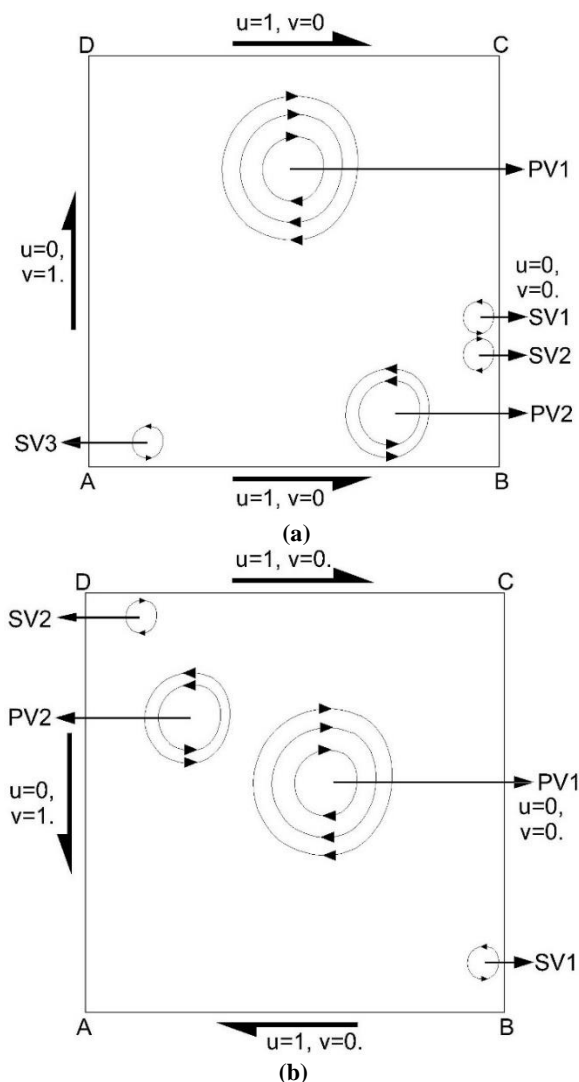


Fig. 1. 2D three-sided lid-driven cavity flow configuration and boundary conditions for (a) case (1) and (b) case (2).

Manuscript received October 26, 2019; revised December 15, 2019.

Abanoub G. Kamel, Eman H. Haraz, and Sarwat N. Hanna are with the Department of Engineering Mathematics and Physics, Faculty of Engineering, Alexandria University, Alexandria 21544, Egypt (e-mail: abanoub.george@alexu.edu.eg, eman.haraz@alexu.edu.eg, sarwat.hanna@alexu.edu.eg).

II. PROBLEM STATEMENT

Consider an incompressible, two-dimensional (2D), time-dependent, and laminar Newtonian internal fluid flow in a square cavity of size (1×1), where, two distinguished unexplored cases of three-sided lid-driven square cavity flow will be investigated as shown in Fig. 1. In case (1) the upper and lower walls are translated to the right whereas the left wall is translated upward and the right wall remains stationary. Moreover, in case (2) the upper wall is translated to the right but the lower wall is translated to the left whereas the left wall is translated downward and the right wall remains stationary. Moreover, the speed magnitude is unity for all moving walls. These movements induce several vortices depending mainly on the Reynolds number (Re) and they are classified as Primary Vortex (PV_x) and Secondary Vortex (SV_x), where the subscript (x) is denoted for the vortex number. The no-slip boundary condition is applied to the right wall in both cases. However, the grid used for (Re = 100) is (151×151) whereas for (Re = 500, 1000, and 2000) is (201×201). The selected Re values are based on a transformation in vortices generation, intense, and location. It is noteworthy that there are another two unexplored configurations for a three-sided lid-driven cavity without repetition. But we decided to simulate the two mentioned cases because they generate more vortices.

III. GOVERNING EQUATIONS

Consider an incompressible, 2D, time-dependent, viscous, and Newtonian fluid flow in a three-sided lid-driven square cavity. The dimensionless governing equations are the continuity (1) and 2D Navier-Stokes (2) and (3) in Cartesian coordinates which are given as follows [14]:

$$\frac{\partial u}{\partial x} + \frac{\partial v}{\partial y} = 0, \quad (1)$$

$$\frac{\partial u}{\partial t} + u \frac{\partial u}{\partial x} + v \frac{\partial u}{\partial y} = -\frac{\partial p}{\partial x} + \frac{1}{\text{Re}} \left(\frac{\partial^2 u}{\partial x^2} + \frac{\partial^2 u}{\partial y^2} \right) \quad (2)$$

$$\frac{\partial v}{\partial t} + u \frac{\partial v}{\partial x} + v \frac{\partial v}{\partial y} = -\frac{\partial p}{\partial y} + \frac{1}{\text{Re}} \left(\frac{\partial^2 v}{\partial x^2} + \frac{\partial^2 v}{\partial y^2} \right) \quad (3)$$

where, (u , v , p , and Re) are the velocity components along (x and y) axes, pressure, and Reynolds number, respectively.

For a two-dimensional flow, the vorticity ω at a certain fluid point is given by

$$\omega = \frac{\partial v}{\partial x} - \frac{\partial u}{\partial y} \quad (4)$$

Defining, the stream function ψ in Cartesian coordinate through

$$u = \frac{\partial \psi}{\partial y}, \quad v = -\frac{\partial \psi}{\partial x} \quad (5)$$

As the difference between two streamlines gives the volumetric flow rate between them and in order to derive the vorticity transport equation, the pressure is eliminated from the momentum equations by cross-differentiation. Differentiating (2) with respect to y and differentiating (3) with respect to x then subtracting the final equation from the earlier one, and by using (5) to replace velocity components

with stream function, we get

$$\frac{\partial \omega}{\partial t} + \frac{\partial \psi}{\partial y} \frac{\partial \omega}{\partial x} - \frac{\partial \psi}{\partial x} \frac{\partial \omega}{\partial y} = \frac{1}{\text{Re}} \left(\frac{\partial^2 \omega}{\partial x^2} + \frac{\partial^2 \omega}{\partial y^2} \right) \quad (6)$$

Now, after the substitution of (5) in (4) the differential form of the elliptic stream function equation, known as Poisson equation (7), is given by

$$\frac{\partial^2 \psi}{\partial x^2} + \frac{\partial^2 \psi}{\partial y^2} = -\omega. \quad (7)$$

Once the stream function has been computed, the velocity components can be found using (5). Equations (4, 5, 6, and 7) are made dimensionless using a reference time, length, and velocity.

IV. NUMERICAL DISCRETIZATION

In order to discretize the computational domain, a structured collocated grid having (n_x) horizontal grid lines and (n_y) vertical grid lines, will be chosen for this problem, where the value of any variable (ω, ψ, u , and v) will be stored at the same point (i, j) and at two different time steps on a five-point stencil. The FDM will be used and Navier-Stokes equations are solved by the ADI scheme which is well established by [14]. However, the forward difference for time discretization and central difference for spatial discretization known as (FTCS) will be applied for the first as well as the second partial derivatives in (6) and (7).

The resulting accuracy from using ADI technique along with FDM will be from the second-order in time and space $O((\Delta t)^2, (\Delta x)^2, \text{ and } (\Delta y)^2)$ and it is unconditionally Stable according to [14]. Therefore, a larger time step can be used. Moreover, the benefit of using the vorticity-stream function form is the decoupling of pressure from velocity as well as guarantee satisfaction of the continuity (1). By solving the vorticity transport equation (6), the value of vorticity can be obtained in the computational domain. The values of the vorticity will then be introduced to the stream function Poisson equation (7). The resulting system of linear equations from the ADI scheme will be solved simultaneously, by means of the Tri-Diagonal Matrix Algorithm (TDMA) known as the Thomas algorithm.

V. BOUNDARY CONDITIONS

Consider the structured collocated grid for a description of the boundary conditions for three physical quantities: velocity, stream function, and vorticity, respectively on the four cavity sides as shown in Table I. Since stream function is constant along a wall, all its derivatives along the wall vanish. Therefore, the stream function Poisson equation (7) reduces to

$$\frac{\partial^2 \psi}{\partial N^2} \Big|_{\text{wall}} = -\omega_{\text{wall}}. \quad (8)$$

where (N) is the normal direction. Moreover, Taylor series expansion has been used so that, the boundary conditions for vorticity (ω) were obtained with truncation error of first order.

TABLE I: BOUNDARY CONDITIONS FOR STREAM FUNCTION, VORTICITY, AND VELOCITY

Cavity side	Physical Quantity		Velocity (u, v)	
	Stream Function (ψ)	Vorticity (ω)	Case (1)	Case (2)
Top wall	$\psi_{i,ny} = 0$	$\omega_{i,ny} = -\frac{\partial^2 \psi}{\partial y^2} = \frac{2(\psi_{i,ny} - \psi_{i,ny-1} - \Delta y * u_{i,ny})}{(\Delta y)^2}$	$u_{i,ny} = 1, v_{i,ny} = 0$	$u_{i,ny} = 1, v_{i,ny} = 0$
Bottom wall	$\psi_{i,1} = 0$	$\omega_{i,1} = -\frac{\partial^2 \psi}{\partial y^2} = \frac{2(\psi_{i,1} - \psi_{i,2} + \Delta y * u_{i,1})}{(\Delta y)^2}$	$u_{i,1} = 1, v_{i,1} = 0$	$u_{i,1} = -1, v_{i,1} = 0$
Left wall	$\psi_{1,j} = 0$	$\omega_{1,j} = -\frac{\partial^2 \psi}{\partial x^2} = \frac{2(\psi_{1,j} - \psi_{2,j} - \Delta x * v_{1,j})}{(\Delta x)^2}$	$u_{1,j} = 0, v_{1,j} = 1$	$u_{1,j} = 0, v_{1,j} = -1$
Right wall	$\psi_{nx,j} = 0$	$\omega_{nx,j} = -\frac{\partial^2 \psi}{\partial x^2} = \frac{2(\psi_{nx,j} - \psi_{nx-1,j} + \Delta x * v_{nx,j})}{(\Delta x)^2}$	$u_{nx,j} = 0, v_{nx,j} = 0$	$u_{nx,j} = 0, v_{nx,j} = 0$

VI. NUMERICAL COMPUTATIONS

The numerical computation of the flow variables u , v , ψ , and ω have been obtained for the current problem with the assistance of computer software. The solution convergence for each Reynolds number (Re) was measured by the residual of the vorticity (9) as indicated in [7], which is given as:

$$R_\omega = \sum_{i=2, j=2}^{i=nx, j=ny} (\omega_{i,j}^{n+1} - \omega_{i,j}^n)^2 \quad (9)$$

where (R_ω) is the vorticity residual and (n) represents the old iteration. However, the convergence criterion is set to (10^{-10}) for each Reynolds number (Re).

VII. NUMERICAL RESULTS

An incompressible, two-dimensional (2D), time-dependent, viscous, Newtonian internal fluid flow in a square cavity of size (1×1) is simulated, in which the upper wall is translated to the right while the other three walls remain stationary. This movement induces a flow characterized by a large Primary Vortex (PV) near the cavity center and smaller secondary vortices namely, Right Secondary Lower Vortex (RSLV), Left Secondary Upper Vortex (LSUV), and Left Secondary Lower Vortex (LSLV) at (Re = 2000). The results were tabulated in Table II.

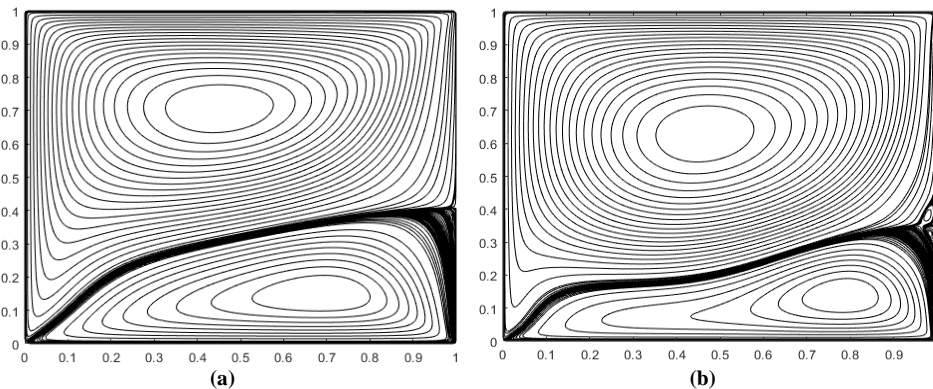
For case (1), Figs. 2 and 3 show the streamlines and vorticity contours, respectively inside the three-sided lid-driven square cavity at different Reynolds numbers specifically (100, 500, 1000, and 2000). Fig. 2 shows the two primary vortices, where PV_1 occurs near the center whereas PV_2 forms near the lower right corner of the cavity. They

also illustrate the three secondary vortices, SV_1 , and SV_2 that form at the lower half of the right wall and they appeared at (Re=500) whereas SV_3 appeared near the lower-left corner at (Re=2000). Additionally, it can be seen from Fig. 2 that the higher the Reynolds number the bigger the size of secondary vortices and PV_1 approaches the cavity center.

Fig. 4 shows the alternation of centerline velocity components' profiles (u and v) along the vertical as well as the horizontal lines, respectively through the center of the three-sided lid-driven square cavity. It is observed that, as Reynolds number increases the profile of the centerline velocity (u) approaches the lower-left corner of the cavity whereas the profile of the centerline velocity (v) approaches the lower right and the upper left corners of the cavity.

TABLE II: PRESENT STUDY VERIFICATION FOR THE ONE-SIDED LID-DRIVEN CAVITY FOR (Re =2000)

Vortex Position	Property	Present	Gupta and Kalita [13]
PV	ψ_{min}	-0.1180	-0.118
	$\omega_{v.c.}$	-1.9477	-----
	x	0.5250	0.5250
	y	0.5500	0.5500
	ψ_{max}	0.0024	0.00241
RSLV	$\omega_{v.c.}$	1.6721	-----
	x	0.8450	0.8375
	y	0.1000	0.1000
	ψ_{max}	7.1188e-4	8.58e-4
	$\omega_{v.c.}$	0.8006	-----
LSLV	x	0.0850	0.0875
	y	0.1050	0.1000
	ψ_{max}	1.1892e-4	1.22e-4
	$\omega_{v.c.}$	0.7774	-----
	x	0.0300	0.0375
LSUV	y	0.8800	0.8875



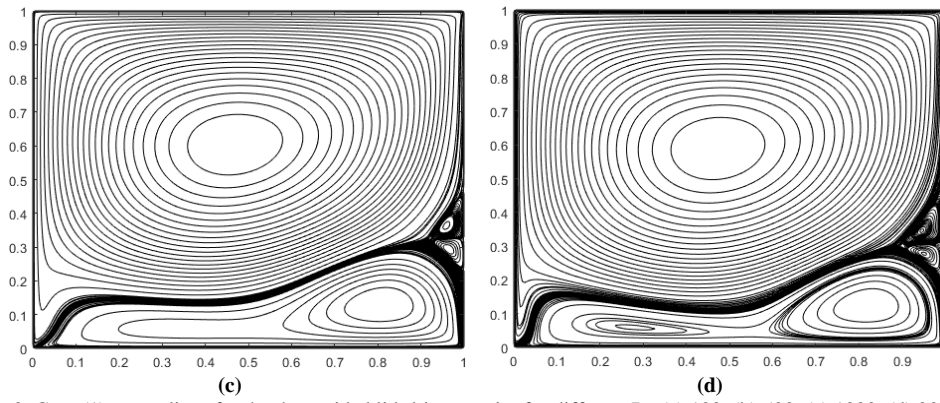


Fig. 2. Case (1) streamlines for the three-sided lid-driven cavity for different Re (a) 100, (b) 500, (c) 1000, (d) 2000.

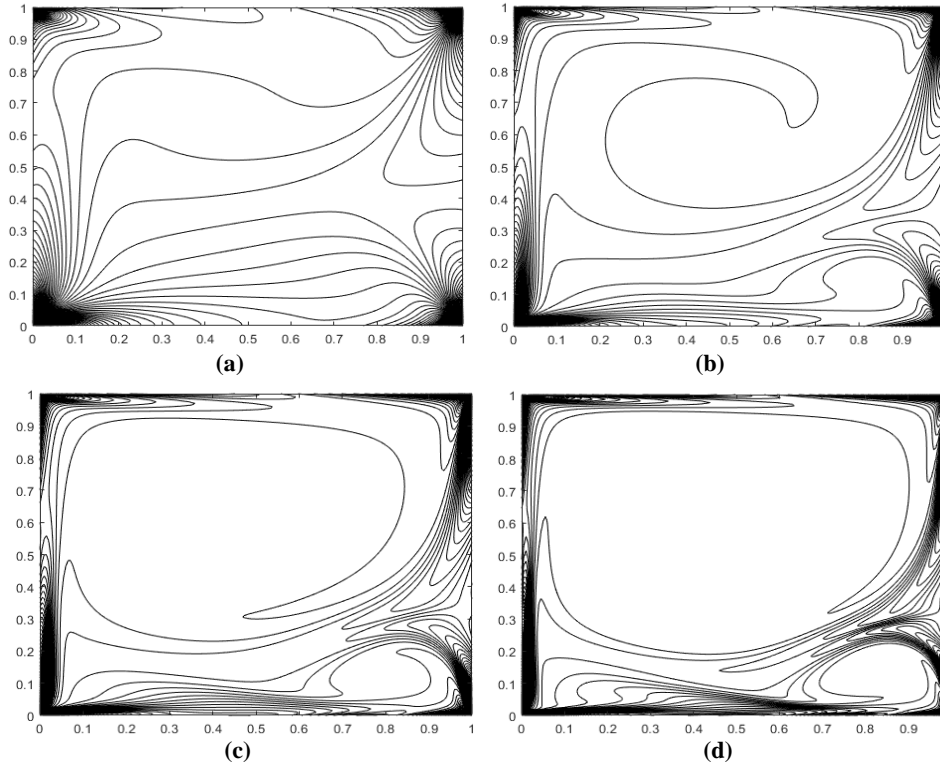


Fig. 3. Case (1) vorticity contours for the three-sided lid-driven cavity for different Re (a) 100, (b) 500, (c) 1000, (d) 2000.

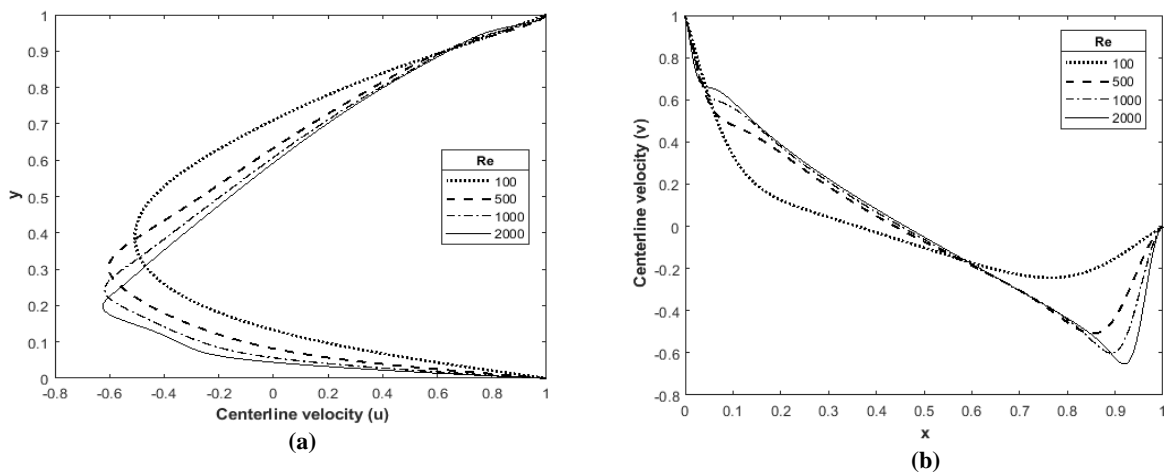


Fig. 4. Case (1) centerline velocity profiles for the three-sided lid-driven cavity flow (a) u, (b) v.

TABLE III: ψ_{min} , ψ_{max} , and $\omega_{v.c}$ VALUES AND LOCATION OF VORTICES' CENTERS FOR THE THREE-SIDED LID-DRIVEN CAVITY FOR CASE (1)

Vortex Position	Property	Reynolds number (Re)			
		100	500	1000	2000
PV ₁	ψ_{min}	-0.1384	-0.1621	-0.1695	-0.1731
	$\omega_{v.c}$	-3.4176	-3.1335	-3.0305	-2.9703
	x	0.4533	0.4650	0.4650	0.4700
	y	0.7067	0.6300	0.6050	0.5900
PV ₂	ψ_{max}	0.0670	0.0607	0.0565	0.0541
	$\omega_{v.c}$	5.4998	7.4313	8.1911	8.8112
	x	0.6867	0.7850	0.8100	0.8200
	y	0.1467	0.1400	0.1300	0.1250
SV ₁	ψ_{max}	-----	2.7712E-5	3.2834E-4	9.6992E-4
	$\omega_{v.c}$	-----	0.3761	1.5538	3.3078
	x	-----	0.9800	0.9600	0.9450
	y	-----	0.3850	0.3650	0.3450
SV ₂	ψ_{min}	-----	-1.2416E-5	-2.5166E-4	-8.2331E-4
	$\omega_{v.c}$	-----	-0.2824	-1.5368	-3.7609
	x	-----	0.9850	0.9650	0.9500
	y	-----	0.3250	0.2950	0.2800
SV ₃	ψ_{max}	-----	-----	-----	0.0222
	$\omega_{v.c}$	-----	-----	-----	9.8357
	x	-----	-----	-----	0.2750
	y	-----	-----	-----	0.0600

It is noticeable from Table III that as the Reynolds number increases the $|\psi_{min}|$ values of PV₁ increase and the ψ_{max} values of PV₂ decrease and this is shown in Fig. 2 by the sizes of PV₁ and PV₂ that increase and decrease, respectively as the Reynolds number increases. Also, the reason for the shrinkage of PV₂ is the formation of secondary vortices SV₁, SV₂, and SV₃.

For case (2), Figs. 5 and 6 show the streamlines and vorticity contours, respectively inside the three-sided lid-driven square cavity for different Reynolds numbers specifically (100, 500, 1000, and 2000). Fig. 5 shows the two primary vortices, where PV₁ occurs near the center whereas PV₂ forms near the left wall of the cavity. They also illustrate the two secondary vortices, SV₁ that forms near the lower

right corner and it appeared at (Re=500) whereas SV₂ appeared near the upper left corner at (Re=1000). Additionally, it can be seen from Fig. 5 that the higher the Reynolds number the bigger the size of secondary vortices and PV₁ approaches the cavity center.

Fig. 7 shows the alternation of centerline velocity components' profiles (u and v) along the vertical as well as the horizontal lines, respectively through the center of the three-sided lid-driven square cavity. It is observed that, as Reynolds number increases the profile of the centerline velocity (u) approaches the upper and lower walls of the cavity whereas the profile of the centerline velocity (v) approaches the upper wall and the lower right corner of the cavity.

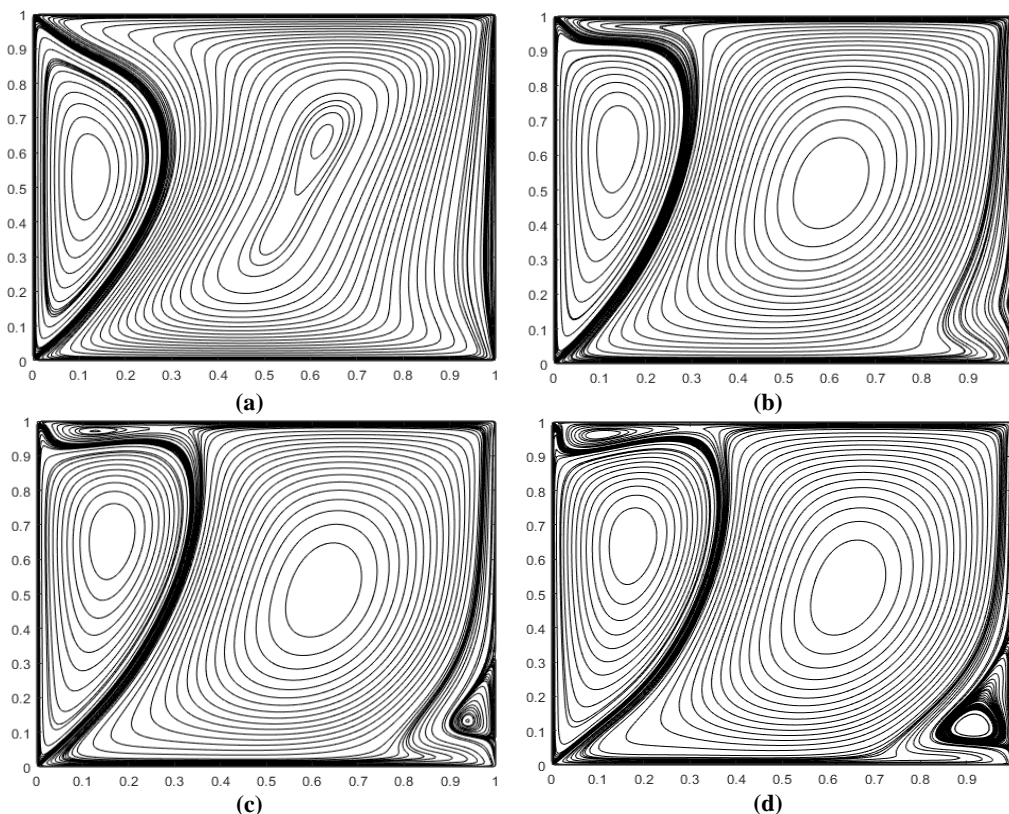


Fig. 5. Case (2) streamlines for the three-sided lid-driven cavity for different Re (a) 100, (b) 500, (c) 1000, (d) 2000.

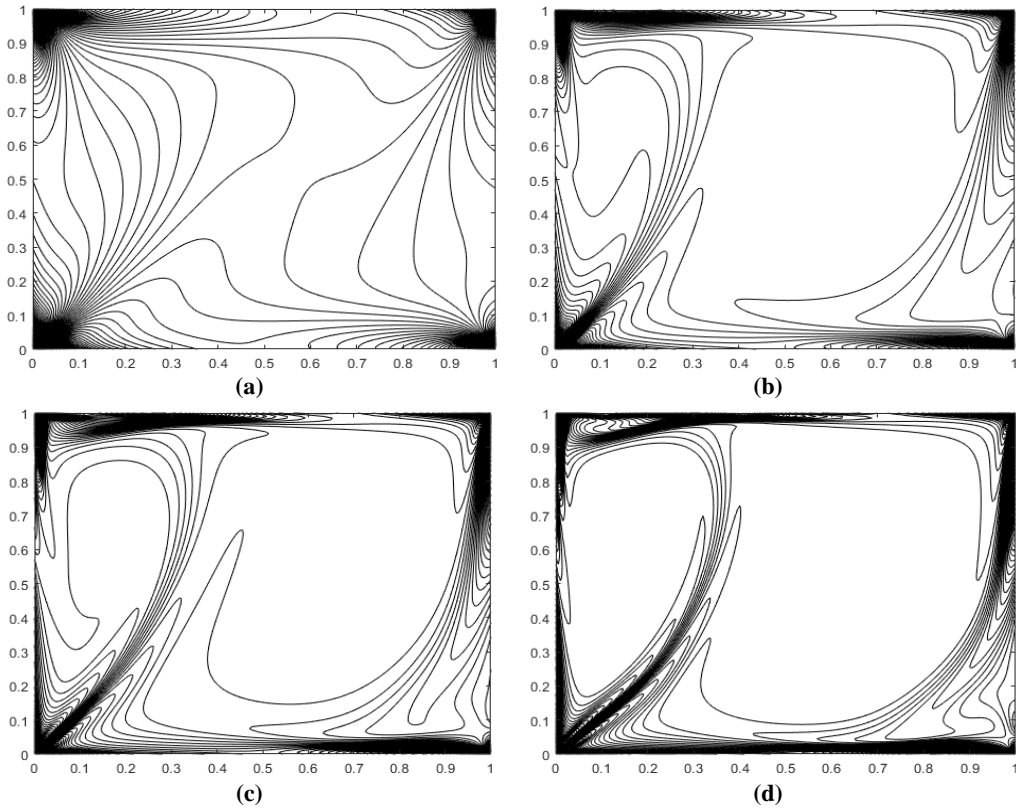


Fig. 6. Case (2) vorticity contours for the three-sided lid-driven cavity for different Re (a) 100, (b) 500, (c) 1000, (d) 2000.

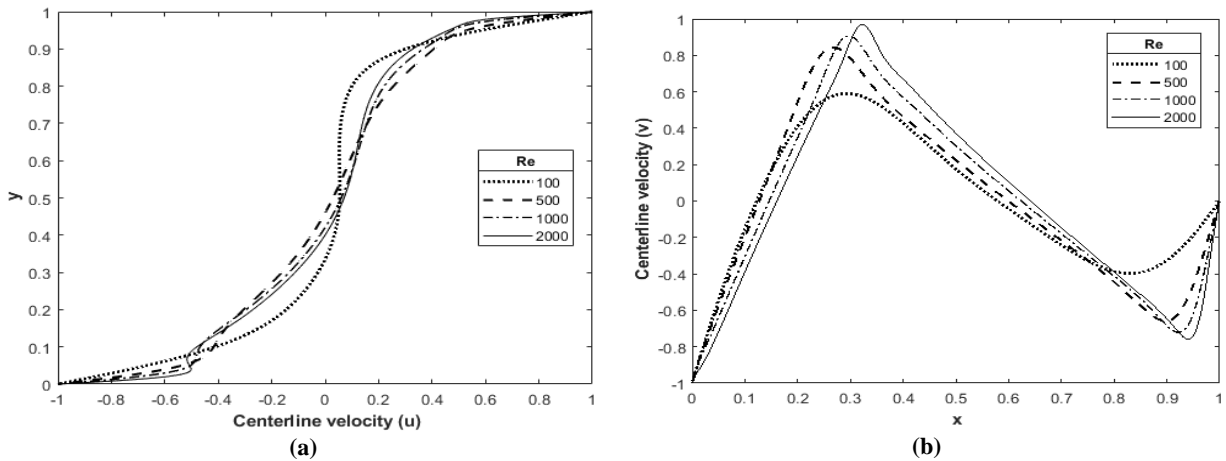


Fig. 7. Case (2) centerline velocity profiles for the three-sided lid-driven cavity flow (a) u, (b) v.

TABLE IV: ψ_{min} , ψ_{max} , and $\omega_{v.c.}$ VALUES AND LOCATION OF VORTICES' CENTERS FOR THE THREE-SIDED LID-DRIVEN CAVITY FOR CASE (2)

Vortex Position	Property	Reynolds number (Re)			
		100	500	1000	2000
PV ₁	ψ_{min}	-0.1044	-0.1422	-0.1418	-0.1396
	$\omega_{v.c.}$	-2.5182	-3.0234	-3.2169	-3.3583
	x	0.6267	0.6050	0.6250	0.6450
	y	0.6400	0.5200	0.5100	0.5200
PV ₂	ψ_{max}	0.0574	0.0668	0.0829	0.0931
	$\omega_{v.c.}$	6.8794	7.5997	7.2145	7.0216
	x	0.1267	0.1400	0.1650	0.1750
	y	0.5333	0.6350	0.6650	0.6500
SV ₁	ψ_{max}	-----	1.4637E-6	0.0011	0.0040
	$\omega_{v.c.}$	-----	0.1468	2.1760	3.5239
	x	-----	0.9950	0.9400	0.9150
	y	-----	0.1700	0.1350	0.1100
SV ₂	ψ_{min}	-----	-----	-0.0131	-0.0154
	$\omega_{v.c.}$	-----	-----	-27.0323	-22.5939
	x	-----	-----	0.1250	0.1050
	y	-----	-----	0.9700	0.9650

Unlike Table III, it is obvious from Table IV that as the Reynolds number increases the $|\psi_{min}|$ values of PV₁

increase but they decrease at (Re = 1000 and 2000) whereas, the ψ_{max} values of PV₂ continued to increase. Additionally,

this is shown in Fig. 5 by the sizes of PV_1 that increase but they decrease at ($Re = 1000$ and 2000) whereas, sizes of PV_2 increase as the Reynolds number increases. Also, the reason for the shrinkage of PV_1 at ($Re = 1000$ and 2000) is the formation of secondary vortices SV_1 and SV_2 combined with the increase in the size of PV_2 .

VIII. CONCLUSION

An incompressible, 2D, unsteady Newtonian fluid flow in a square cavity is simulated in this study using FDM and ADI technique. The one-sided lid-driven cavity is examined at ($Re = 2000$) in order to validate the results and they are in a very good agreement with published results in the literature. Two distinguished unexplored cases of the three-sided lid-driven cavity have been investigated. In this work, the speed magnitude is unity for all moving walls. It is observed from the streamlines' Figs. that as Reynolds number increases, the main primary vortex approaches the cavity center and the secondary vortices get bigger in size and strength. Also, in case (1) the sizes of PV_1 and PV_2 increase and decrease, respectively as the Reynolds number increases. On the other hand, in case (2) the sizes of PV_1 increase but they decrease at ($Re = 1000$ and 2000) whereas, the sizes of PV_2 increase as the Reynolds number increases. As the current numerical solution for the flow established in the three-sided lid-driven square cavity like no other, these outcomes offer a vital source to researchers to verify their outcomes. The MATLAB® code used in this study can be used to solve several fluid flow problems with accurate results, these problems may be either internal or external flows such as channel flow or flow over obstacles with simple geometry.

CONFLICT OF INTEREST

The authors declare no conflict of interest.

AUTHOR CONTRIBUTIONS

Abanoub G. Kamel conducted the research and wrote the paper; Eman H. Haraz and Sarwat N. Hanna analyzed the results; all authors had approved the final version.

REFERENCES

- [1] P. Gaskell, J. Summers, H. Thompson, and M. Savage, "Creeping flow analyses of free surface cavity flows," *Theoretical and Computational Fluid Dynamics*, vol. 8, no. 6, pp. 415-433, 1996.
- [2] C. K. Aidun, N. Triantafillopoulos, and J. Benson, "Global stability of a lid-driven cavity with throughflow: Flow visualization studies," *Physics of Fluids A: Fluid Dynamics*, vol. 3, no. 9, pp. 2081-2091, 1991.
- [3] E. Mitsoulis, S. Marangoudakis, M. Spyrtos, T. Zisis, and N. A. Malamataris, "Pressure-driven flows of Bingham plastics over a square cavity," *Journal of Fluids Engineering*, vol. 128, no. 5, pp. 993-1003, 2006.
- [4] N. Alleborn, H. Raszillier, and F. Durst, "Lid-driven cavity with heat and mass transport," *International Journal of Heat and Mass Transfer*, vol. 42, no. 5, pp. 833-853, 1999.
- [5] P. Zdanski, M. Ortega, and N. G. Fico Jr, "Numerical study of the flow over shallow cavities," *Computers and Fluids*, vol. 32, no. 7, pp. 953-974, 2003.
- [6] Z. Cao and M. N. Esmail, "Numerical study on hydrodynamics of short-dwell paper coaters," *AIChE Journal*, vol. 41, no. 8, pp. 1833-1842, 1995.
- [7] P. Ghadimi, M. Y. Fard, and A. Dashtimanesh, "Application of an iterative high order difference scheme along with an explicit system solver for solution of stream function-vorticity form of navier-stokes

equations," *Journal of Fluids Engineering*, vol. 135, no. 4, p. 041401, 2013.

- [8] H. C. Kuhlmann and F. Romanò, "The lid-driven cavity," in *Computational Modelling of Bifurcations and Instabilities in Fluid Dynamics*: Springer, 2019, pp. 233-309.
- [9] P. Shankar and M. Deshpande, "Fluid mechanics in the driven cavity," *Annual Review of Fluid Mechanics*, vol. 32, no. 1, pp. 93-136, 2000.
- [10] D. W. Peaceman and J. Rachford, Henry H, "The numerical solution of parabolic and elliptic differential equations," *Journal of the Society for Industrial and Applied Mathematics*, vol. 3, no. 1, pp. 28-41, 1955.
- [11] U. Ghia, K. N. Ghia, and C. Shin, "High-Re solutions for incompressible flow using the navier-stokes equations and a multigrid method," *Journal of Computational Physics*, vol. 48, no. 3, pp. 387-411, 1982.
- [12] E. Wahba, "Multiplicity of states for two-sided and four-sided lid driven cavity flows," *Computers and Fluids*, vol. 38, no. 2, pp. 247-253, 2009.
- [13] M. M. Gupta and J. C. Kalita, "A new paradigm for solving Navier-Stokes equations: streamfunction-velocity formulation," *Journal of Computational Physics*, vol. 207, no. 1, pp. 52-68, 2005.
- [14] K. A. Hoffmann and S. T. Chiang, *Computational Fluid Dynamics Volume I Engineering Education System*, 2000.

Copyright © 2020 by the authors. This is an open access article distributed under the Creative Commons Attribution License which permits unrestricted use, distribution, and reproduction in any medium, provided the original work is properly cited ([CC BY 4.0](https://creativecommons.org/licenses/by/4.0/)).



Abanoub G. Kamel was born in Alexandria, Egypt in 1993 and earned his B.Sc. degree with honor in mechanical engineering from the Faculty of Engineering, Alexandria University, Egypt in 2016. He is currently pursuing an M.Sc. degree in computer simulation engineering with the Department of Engineering Mathematics and Physics, Faculty of Engineering, Alexandria University, Egypt.

He worked as an HVAC design engineer at a consultant office for Electromechanical works, also he is currently working as a tenured Teaching Assistant at Faculty of Engineering, Alexandria University. His research interest includes Fluid Dynamics, Modeling and simulation of Mechanical Systems, Heat and Mass Transfer, Sustainable Energy.

Eng. Kamel is a member of Egyptian Engineering Syndicate.



Eman H. Haraz was born in Damanhur, Egypt in 1976. She got her B.Sc. in textile engineering with honor 1999 from the Faculty of Engineering at Alexandria University. M.Sc. in engineering mathematics (dynamical investigation and Vibration of twisting machines) in 2006 Alexandria University. Ph.D. in engineering mathematics (robot dynamics and optimization) Alexandria University in 2013.

She is currently an assistant professor in the Department of Engineering Mathematics and Physics, Faculty of Engineering, Alexandria University. She has an interest in modeling and simulation of dynamical systems and optimization research.

Sarwat N. Hanna was born in Damnhour, Egypt, in 1943. He received his B. Sc. in electrical-power engineering from Alexandria University, Egypt (1966), He received his B. Sc. in applied mathematics from Alexandria University, Egypt (1972), He received his M. Sc. in electrical engineering, from Alexandria University, Egypt (1973), He revised his Dip. D., theoretical physics, Faculty of Science, University of Konstanz, Germany (West) (1978) and Dr.rer.nat., Statistical Mechanics, Faculty of Science, University of Konstanz, Germany (West) (1982).

Professor emeritus of App. Mathematics, Department of Engineering Mathematics and Physics, Faculty of Engineering, Alexandria University, Egypt since (2003).